Nonlinear current response of Weyl semimetals to a strong dc-ac electric field in the ultraquantum regime

Zhigang Wang, Zhen-Guo Fu, Ping Zhang,* and Wei Zhang†
Institute of Applied Physics and Computational Mathematics, Beijing 100088, China

(Received 7 October 2021; accepted 4 May 2022; published 17 May 2022)

The linear charge transport properties of Weyl semimetals, such as negative magnetoresistance related to chiral anomaly, have been studied extensively. In this work, the *nonlinear* current response of Weyl semimetals to a strong dc-ac electric field in the ultraquantum regime with a strong magnetic field is explored by employing a *nonperturbative* treatment based on the stochastic Liouville equation. Our systematic studies of nonlinear charge transport for two types of ac fields (the cosinusoidal electric field and the periodic pulsed field) have revealed extraordinary modulation of nonlinear current response by the ac fields. For the case with the cosinusoidal electric field, we find the following: (i) in the high-frequency regime, dynamic localization (vanishing of current) and quasienergy band collapse occur under a suitable condition of $J_0(\frac{eE_Ad}{\hbar\omega_0})=0$, where J_0 is the Bessel function with E_A and ω_0 being the strength and frequency of the ac field, and d denoting the lattice constant of Weyl semimetals; and (ii) in the intermediate- and low-frequency regimes, the multiple-photon-assisted transport leads to extremal values of current responses whose patterns can be tuned by the magnetic field. As for the pulsed electric field, our results show that (i) the dynamic localization and quasienergy band collapse appear under a different condition of $\cos(\frac{eE_Ad}{\hbar\omega_0})=0$; and (ii) the influence of the ac field on the current response disappears when $\frac{eE_Ad}{\hbar\omega_0}=m\pi$, with m being an integer. The experimental conditions are also discussed and the predicted nonlinear transport effects could be observed in experiments.

DOI: 10.1103/PhysRevB.105.205303

I. INTRODUCTION

Nowadays, two-dimensional (2D) and three-dimensional (3D) Dirac materials, such as graphene [1,2], 3D topological insulators [3,4], and Weyl semimetals [5–16], have attracted more and more attention in the field of condensed-matter physics for the abundant topological properties they offer. Especially, Wan and his collaborators have predicted $Y_2Ir_2O_7$ to be a Weyl semimetal [6]. A family of nonmagnetic materials including TaAs, TaP, NbAs, and NbP have also been demonstrated as type-I Weyl semimetals, in which inversion symmetry is broken but time-reversal symmetry holds, and a pair of upright Weyl cones with opposite chirality are pinned at Fermi level [12]. More recently, a series of Weyl semimetals has been theoretically proposed and realized in experiments. According to the geometry of the Fermi surfaces, Weyl semimetals have been generalized into type-II and type-III. Differing from the type-I Weyl semimetals, the Weyl cones in type-II Weyl semimetals are overtilted, and the corresponding Fermi surface is composed of touched electron-hole pockets [13]. Furthermore, the Fermi surface of type-III Weyl semimetals consists of two-electron or two-hole pockets touching at a multi-Weyl cone [14].

Remarkably different from conventional electronic structures, which possess a parabolic low-energy dispersion relationship near the Fermi level, the low-energy states near the Weyl nodes of Weyl semimetals are characterized by a Weyl Hamiltonian with linear gapless dispersions. The Weyl nodes act as monopoles in momentum space with topological charges. The geometry and topology of Weyl semimetals related to the Berry phase and the monopole charge lead to novel physical consequences, such as Fermi arc surface states, the magnetotransport related to chiral anomaly, the anomalous Hall effect, and axion electrodynamics [5].

External fields have great impact on the electronic dynamics of Weyl semimetals. In the presence of a magnetic field, interesting physical effects, such as magnetothermal conductivity [17], the magneto-optical response [18,19], the 3D Hall effect [20], the chiral magnetic effect [21–24], and the nonlinear Hall effect [25–27] have been theoretically and experimentally explored. The magnetic field not only changes the band structure (formation of Landau levels) but also affects the scattering time [28–32], which is crucial in charge transport. In particular, experiments and theory (based on either quantum theory or the semiclassical approach with the Berry-phase effect taken into account [33,34]) have revealed the magnetotransport property related to a chiral anomaly [28–32,35–44]. The dependence of magnetoconductivity of Weyl semimetals on the external magnetic field B exhibits interesting features. For instance, in the weak magnetic field regime, magnetoconductivity is proportional to B^2 [31,41,42]; while in the quantum regime with a strong magnetic field, a linear dependence of magnetoconductivity on B has been uncovered [39,42]. Most recently, a unified picture of the magnetotransport of Weyl semimetals covering the weak and strong magnetic field regimes has been developed, and a

*zhang_ping@iapcm.ac.cn
†zhang_wei@iapcm.ac.cn

transition from quadratic magnetoconductivity at weak magnetic fields to linear magnetoconductivity at high magnetic fields has been theoretically obtained [45].

Furthermore, recent studies have indicated that ac fields have an important impact on the quasienergy spectrum and the electric transport in Weyl semimetals as well as other Dirac systems [46–60]. For example, despite the absence of an external magnetic field, a dynamic gap in the Dirac cone of the graphene system can be opened under the application of an ac field and the so-called photovoltaic Hall effect may be realized [46–48]. Ma *et al.* and Chan *et al.* studied the photon current in Weyl semimetals [49,50]. The topological properties of light-induced Floquet-Weyl semimetals have also been extensively studied [52–56]. It is noticed that because the time-reversal symmetry is broken by a circularly polarized laser field, distinct shifts in the spectrum of each Weyl cone in Floquet-Weyl semimetals are generated. Kundu *et al.* investigated the Floquet topological transitions [60].

Most of the studies on charge transport mentioned above focused on the linear response of Weyl semimetals to weak dc fields. Recently, the nonlinear current response of Weyl semimetals to strong dc electric fields in the ultraquantum regime have been investigated, and the nonmonotonic dependence of current on the electric field and the optimal condition for the highest current response have been uncovered [61]. The nonlinear response may not only provide an important alternative approach to testify various extraordinary exotic properties, such as Fermi arcs and the chiral anomaly involved in Weyl semimetals, but may also provide instructive guidance on designing nanodevices based on Weyl semimetals. Due to the importance in both the perspectives of basis physics and potential applications of Weyl semimetals in nanodevice fields, it is interesting and timely necessary to carry out a theoretical analysis of the nonlinear current response of Weyl semimetals to the dc-ac electric field in the ultraquantum regime with a strong magnetic field. From this aspect, we take a step further to investigate this problem by employing a nonperturbative approach based on the stochastic Liouville equation (SLE) [62–66]. Our current work is remarkably different from many studies that have focused on generating the Floquet-Weyl semimetal phase by time-dependent fields or the current response based on perturbative formalism.

The systematic theoretical studies in this work reveal several interesting features in the nonlinear charge transport driven by dc-ac fields. Two types of ac fields, the cosinusoidal electric field and the periodic pulsed field, are considered in our Weyl semimetal systems. We find that in the high-frequency regime, the ac fields bring about interesting renormalization effects of current. Explicitly, for the cosinusoidal electric field with high frequency, the long-time averaged current can be derived as $\langle j\rangle = \langle j\rangle|_{E_A=0} J_0^2(\bar{\omega}_A)$, where $\langle j\rangle|_{E_A=0}$ is the current response to a pure dc field, and $J_0(\bar{\omega}_A)$ is the zeroth Bessel function. Here, $\bar{\omega}_A = \frac{eE_A d}{\hbar\omega_0}$, with d being the lattice constant of Weyl semimetals. Dynamic localization (current suppression) and quasienergy band collapse appear under the condition of $J_0(\bar{\omega}_A) = 0$. In the intermediate- and low-frequency regimes, multiple-photon-assisted transport leads to multiple-resonance patterns in the nonlinear current responses. For the periodic pulsed field, $\langle j\rangle = \langle j\rangle|_{E_A=0}\cos^2\bar{\omega}_A$. It is clear that the corresponding dynamic localization and quasienergy band collapse induced by the periodic pulsed field occur under a different condition of $\cos\bar{\omega}_A = 0$. Furthermore, the modulation from the periodic pulsed field disappears when $\frac{eE_A d}{\hbar\omega_0} = m\pi$, with m being an integer. Moreover, the experimental conditions to observe the theoretical predictions shown in this paper are briefly addressed.

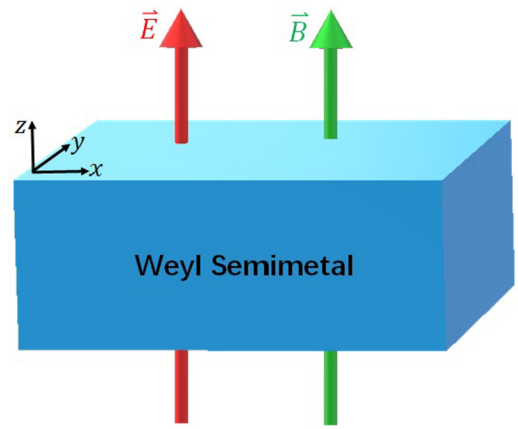

FIG. 1. The scheme of a Weyl semimetal under the external electric field and the magnetic field, which are parallel to the z direction.

II. THEORETICAL FORMULISM: THE HAMILTONIAN AND THE SLE

We start from the minimal cubic lattice model of Weyl semimetals $H(\mathbf{k}) = H_0(\mathbf{k}) + H_1(\mathbf{k})$ [67]. $H_0(\mathbf{k})$ describes an electronic dynamics in a cubic lattice with the lattice constant d, which is given by

$$H_0(\mathbf{k}) = \frac{\hbar v}{d}\{\sigma_z\otimes[s_x\sin(k_y d) - s_y\sin(k_x d)] + \sigma_y\otimes\sin(k_z d)\}, \tag{1}$$

with σ and $\mathbf{s}$ being the Pauli matrices in orbital and spin space, respectively. The low-energy effective Hamiltonian around the three-dimensional (3D) Dirac points (0,0,0) and $(0, 0, \pi)$ can be written as the usual form $H_\chi(\mathbf{k}) = \chi\hbar v\mathbf{k}\cdot\sigma$, with $\chi = \pm 1$ denoting two kinds of chirality and $\mathbf{k}$ being the wave vector relative to the Dirac points. The energy spectra around the 3D Dirac points can be readily obtained as $E_{\pm,\chi}(\mathbf{k}) = \chi\hbar v k$. The other time-reversal symmetry-breaking perturbation term $H_1(\mathbf{k})$ is of the form $H_1(\mathbf{k}) = \frac{\hbar v}{d} b\otimes s_z$, with $|b| < 1$. Then the Weyl semimetal emerges with the Weyl points at $\pm\bar{k}_z = \pm\frac{1}{d}\arcsin$ (b) and the effective Fermi velocity $v_F = v\sqrt{1-b^2}$.

We consider both a magnetic field and a dc-ac electric field along the z direction, i.e., $\mathbf{B} = B\hat{z}$ and $\mathbf{E} = E\hat{z}$. The scheme of the Weyl semimetal under the external electric field and the magnetic field is shown in Fig. 1. In this paper we are interested in the nonlinear current response along the $\hat{z}$ direction. By taking the low-energy linear approximation along the $\hat{x}-\hat{y}$ plane and introducing the Landau ladder operators $a^\dagger = \frac{l_B}{\sqrt{2}}(\Pi_x - i\Pi_y)$ and $a = \frac{l_B}{\sqrt{2}}(\Pi_x + i\Pi_y)$, with $\Pi = (\Pi_x, \Pi_y, 0) = \mathbf{k} + e\mathbf{A}$, $\mathbf{A} = (0, Bx, 0)$, and $l_B = \sqrt{\hbar/eB}$ being the magnetic length, we can obtain the effective

Hamiltonian as

$$\mathcal{H}(k_z) = H(k_z) - eEzI_{4\times4}, \tag{2}$$

with

$$H = \hbar v \begin{pmatrix} \frac{b}{d} & i\frac{\sqrt{2}a}{l_B} & -i\frac{\sin(k_z d)}{d} & 0 \\ -i\frac{\sqrt{2}a^\dagger}{l_B} & -\frac{b}{d} & 0 & -i\frac{\sin(k_z d)}{d} \\ i\frac{\sin(k_z d)}{d} & 0 & -\frac{b}{d} & i\frac{\sqrt{2}a}{l_B} \\ 0 & i\frac{\sin(k_z d)}{d} & -i\frac{\sqrt{2}a^\dagger}{l_B} & \frac{b}{d} \end{pmatrix}. \tag{3}$$

In the following we abbreviate k_z as k for the convenience of expression.

It is seen that the magnetic field discretizes the continuum energy spectra into a series of Landau levels (LLs), and the energy spectra are given by

$$\varepsilon_{n,s}(\chi) = \begin{cases} s\hbar v\sqrt{d^{-2}[b \pm \sin(kd)]^2 + 2n(l_B)^{-2}}, & n \neq 0, \\ -\chi(\hbar v/d)[\sin(kd) \pm b], & n = 0. \end{cases} \tag{4}$$

In the ultraquantum regime, both the chemical potential μ and the temperature $k_B\mathcal{T} \equiv 1/\beta$ are small compared to the energy difference between the zeroth level and the first LLs, i.e., $\mu, 1/\beta < \sqrt{2}\hbar v/l_B$. In this case, only the chiral branches of the spectrum ($n = 0$ LLs) are occupied by electrons, which contribute to the current.

The dc-ac electric field is given by

$$\boldsymbol{E} = [E_D + E_A P(\omega_0 t)]\hat{z}, \tag{5}$$

with E_D being the dc field strength, and E_A and ω_0 being the strength and the frequency of the ac field. $P(\omega_0 t)$ is a periodic function. In the present work, we consider two types of ac electric fields: the cosinusoidal electric field and the periodic pulsed field. Explicitly,

$$P(\omega_0 t) = \cos(\omega_0 t) \tag{6}$$

for the cosinusoidal electric field and

$$P(\omega_0 t) = 2\sum\nolimits_{m=0}^{\infty}(-1)^m\delta(\omega_0 t - m\pi) \tag{7}$$

for the periodic pulsed field. The periodic pulsed field in Eq. (7) can be considered as a sum of the trigonometric functions with different weights, i.e., $\sum_m(-1)^m\delta(\omega_0 t - m\pi) = \sum_n c_n\cos(n\omega_0 t)$.

To explore the nonlinear transport of Weyl semimetals in the ultraquantum regime, we apply a nonperturbative approach based on the SLE [64], which has been successfully used to study the Zener transitions between dissipative Bloch bands [65]. Within a constant relaxation rate approximation, the SLE for the density matrix ρ is expressed as [64]

$$i\hbar\frac{\partial\rho}{\partial t} = [H, \rho(t)] - i\Gamma[\rho(t) - \rho_{\mathcal{T}}]. \tag{8}$$

Here, $\rho(t)$ is the density matrix with matrix elements $\rho^{N_i,N_j}(t) = \langle N_i|\hat{\rho}|N_j\rangle$. The density operator is defined as $\hat{\rho} = \psi\psi^\dagger = \sum_{N_1,N_2}^{N_{\max}} c_{N_1}c_{N_2}^*|N_1\rangle\langle N_2|$, with $\psi = \sum_N^{N_{\max}} c_N|N\rangle$ being the wave function of electrons under the basis of $\{|N\rangle\} = \{|n, s, \chi\rangle\}$. $\rho_{\mathcal{T}}$ is the Fermi-Dirac equilibrium distribution at temperature $\mathcal{T}$, which is written as $\rho_{\mathcal{T}}^{N_i}(k) = \{\exp[\beta\varepsilon_{N_i}(k)] + 1\}^{-1}$ with the chemical potential set to $\mu = 0$ for simplicity. Γ describes the relaxation of the off-diagonal elements of $\rho(t)$ through dephasing [61,64]. In our case, the intervalley scattering dominates and the k dependence of the scattering time can be neglected due to the splitting of the Weyl points in momentum space. Thus, there is no change of the main physics by using the relaxation time approximation, which has also been applied in previous studies of magnetotransport in Weyl semimetals [17,36]. After some derivations, Eq. (8) is rewritten as

$$\frac{\partial\rho^{N_i;N_j}}{\partial\bar{t}} - [\bar{\omega}_D + \bar{\omega}_A P(\bar{t})]\frac{\partial\rho^{N_i;N_j}}{\partial\bar{k}} = F(N_i;N_j) - \bar{\alpha}\left[\rho^{N_i;N_j} - \rho_{\mathcal{T}}^{N_i}\delta_{N_iN_j}\right], \tag{9}$$

in which we have employed the dimensionless parameters $\bar{k} = kd$, $\bar{t} = \omega_0 t$, $\bar{\varepsilon}_{N_i}(\bar{k}) = \varepsilon_{N_i}(k)/\hbar\omega_0$, $\bar{\beta} = \beta\hbar\omega_0$, $\bar{\omega}_{D(A)} = eE_{D(A)}d/\hbar\omega_0$, and $\bar{\alpha} = 1/\tau\omega_0$, with τ representing the relaxation time. In Eq. (9), $F(N_i;N_j)$ is a very complex function and has relation with the other LLs (same n index and different χ and s).

In the present work, we consider Weyl semimetals in the ultraquantum regime with a strong magnetic field, so that only the lowest LLs are occupied by electrons. Namely, only $|N_1\rangle \equiv |n = 0, \chi = 1\rangle$ and $|N_2\rangle \equiv |n = 0, \chi = -1\rangle$ are considered in Eq. (9). The general case for any B including the LLs with $n \neq 0$ terms is left for future study. We briefly denote $|N_{1(2)}\rangle$ as $|\chi = \pm1\rangle$ in the following. Based on this consideration, Eq. (9) is simplified as

$$\frac{\partial\rho_{\chi;\chi}}{\partial\bar{t}} - [\bar{\omega}_D + \bar{\omega}_A P(\bar{t})]\frac{\partial\rho_{\chi;\chi}}{\partial\bar{k}} = -\bar{\alpha}\left[\rho_{\chi;\chi} - \rho_{\mathcal{T}}^{\chi}\right], \tag{10}$$

$$\frac{\partial\rho^{\chi;\bar{\chi}}}{\partial\bar{t}} - [\bar{\omega}_D + \bar{\omega}_A P(\bar{t})]\frac{\partial\rho^{\chi;\bar{\chi}}}{\partial\bar{k}} = 0. \tag{11}$$

As a result, the analytical expression of $\rho_{\chi;\chi}$ is given by

$$\rho^{\chi;\chi} = e^{-\bar{\alpha}\bar{t}}\left\{\rho_{\mathcal{T}}^{\chi}[\bar{k} + \bar{\omega}_D\bar{t} + f(\bar{t})] + \bar{\alpha}\int_0^{\bar{t}} d\bar{t}' e^{\bar{\alpha}\bar{t}'}\rho_{\mathcal{T}}^{\chi}[\bar{k} + \bar{\omega}_D(\bar{t} - \bar{t}') + f(\bar{t}) - f(\bar{t}')]\right\}, \tag{12}$$

where

$$f(x) = \bar{\omega}_A\int_0^x dx' P(x'). \tag{13}$$

Substituting Eqs. (6) and (7) into Eq. (13), one can easily find $f(\bar{t}) = \bar{\omega}_A\sin\bar{t}$ for the cosinusoidal field, and

$$f(\bar{t}) = \begin{cases} \bar{\omega}_A, & \text{for } 2m\pi \leqslant \bar{t} \leqslant (2m+1)\pi, \\ -\bar{\omega}_A, & \text{for } (2m+1)\pi \leqslant \bar{t} \leqslant 2(m+1)\pi, \end{cases} \tag{14}$$

for the periodic pulsed field, respectively. The sketch map of $f(\bar{t})$ is shown in Fig. 2. Finally, the long-time averaged current is given by

$$\langle j\rangle = \lim_{\bar{T}\to\infty}\frac{1}{2\pi\bar{T}}\int_0^{\bar{T}} d\bar{t}\int_{-\pi}^{\pi} d\bar{k}\, j(\bar{k}, \bar{t}), \tag{15}$$

where

$$j(\bar{k}, \bar{t}) = eg\sum_{s,\chi}\frac{\partial\varepsilon_0^{s,\chi}}{\hbar\partial\bar{k}}\rho_{\chi;\chi}(\bar{k}, \bar{t}) = egv_F\cos\bar{k}\rho_-(\bar{k}, \bar{t}), \tag{16}$$

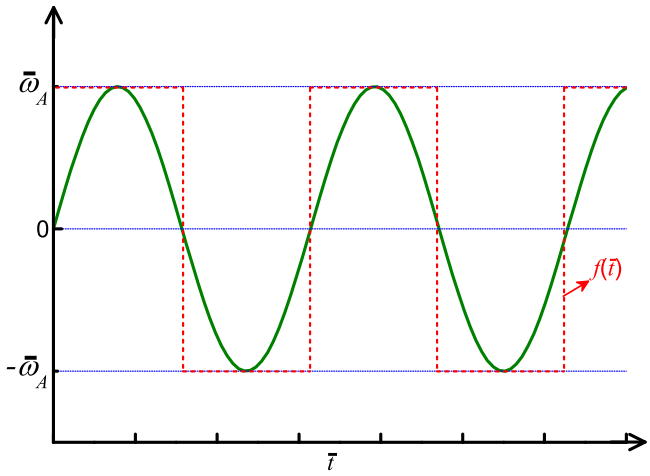

FIG. 2. The sketch map of the function $f(\bar{t})$ in our analytical derivation. The green solid line and the red dashed line represent the $f(\bar{t})$ corresponding to the ac fields of the trigonometric function [Eq. (6)] and the periodic pulse [Eq. (7)], respectively.

with $v_F = v\sqrt{1-b^2}$ being the Fermi velocity, $\rho_- = \rho^{1;1} - \rho^{\bar{1};\bar{1}}$, and $g = \frac{1}{4\pi l_B^2 d}$ being the degree of degeneracy for Weyl fermions.

III. RESULTS AND DISCUSSIONS

A. Nonlinear charge transport modulated by the cosinusoidal electric field

In this subsection, we study the current response to the dc-ac electric field of the form $[E_D+E_A\cos(\omega_0 t)]\hat{z}$. By using Eqs. (12), (13), (15), and (16), the long-time averaged current is derived as

$$\langle j\rangle = egv_F\frac{\bar{\alpha}}{2\pi}\lim_{\bar{T}\to\infty}\frac{1}{\bar{T}}\int_0^{\bar{T}}d\bar{t}\int_0^{\bar{t}}d\bar{t}'Z(\bar{t},\bar{t}'), \tag{17}$$

where $Z(\bar{t},\bar{t}')$ is expressed as

$$Z(\bar{t},\bar{t}') = \mathrm{Re}\left[e^{\bar{\alpha}(\bar{t}'-\bar{t})-is}\int_{s-\pi}^{s+\pi}d\bar{k}e^{i\bar{k}}\tanh\left(\frac{\bar{\beta}\sin\bar{k}}{2}\right)\right], \tag{18}$$

with $s = \bar{\omega}_D(\bar{t}-\bar{t}')+\bar{\omega}_A(\sin\bar{t}-\sin\bar{t}')$. At zero temperature, i.e., $\bar{\beta}\to\infty$, the analytical expression of the long-time averaged current can be obtained as

$$\langle j\rangle = \frac{2\hbar egv_F}{\pi\tau}\sum_{m=-\infty}^{\infty}(-1)^m J_m^2\left(\frac{eE_Ad}{\hbar\omega_0}\right) \times\frac{eE_Dd+m\hbar\omega_0}{(\hbar/\tau)^2+(eE_Dd+m\hbar\omega_0)^2}, \tag{19}$$

where $J_m(z)$ is the mth-order Bessel function of the first kind. During the derivation, we have used the relationships $i = \frac{1}{4}\int_{s-\pi}^{s+\pi}d\bar{k}e^{i\bar{k}}\tanh[\frac{\bar{\beta}\sin\bar{k}}{2}]_{\bar{\beta}\to\infty}$ and $e^{iz\cos x} = J_0(z)+2\sum_{m=1}^{\infty}i^m J_m(z)\cos(mx)$. Equation (19) is the main result of this work. It is clear that $\langle j\rangle = 0$, when $E_D = 0$ as it should be; while in the absence of the ac field ($E_A = 0$), we have

$$\langle j\rangle|_{E_A=0} = \frac{2egv_F}{\pi}\frac{eE_Dd\hbar/\tau}{(\hbar/\tau)^2+(eE_Dd)^2}, \tag{20}$$

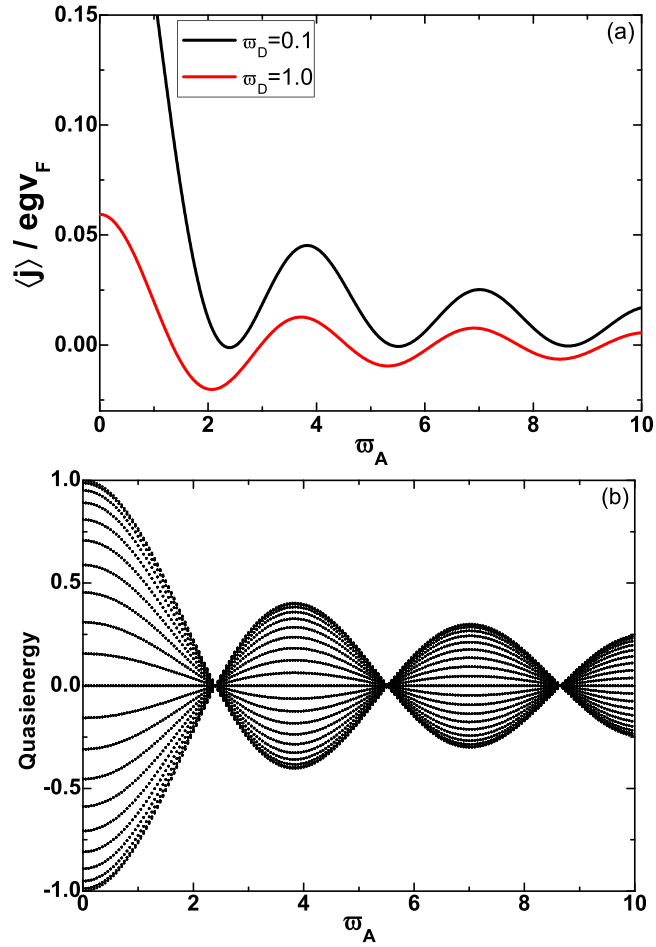

FIG. 3. (a) The current response $\langle j\rangle$ (in unit of egv_F) as a function of $\bar{\omega}_A = edE_A/\hbar\omega_0$. The parameters are $\omega_0 = 2$ THz, $\bar{\alpha} = 1/\tau\omega_0 = 0.2$, and $\bar{\omega}_D = edE_D/\hbar\omega_0 = 0.1, 1.0$. (b) The quasienergy spectrum (in units of $\hbar v/d$) as a function of $\bar{\omega}_A$. $\bar{\omega}_D = 0.1$. The other parameters are the same as those in panel (a).

which is just the nonlinear current response to the pure dc field. Furthermore, for the linear response to the weak dc electric field, Eq. (20) reduces to the well-known result of the linear current response in the ultraquantum regime $\langle j\rangle|_{E_A=0}\to\frac{e^2v_F\tau E_D}{4\pi^2\hbar l_B^2}$ as a consequence of chiral anomaly [28,39].

1. Nonlinear charge transport modulated by the cosinusoidal electric field I: Band collapse and dynamic localization

The dependence of the current $\langle j\rangle$ on the ac field displayed in Fig. 3(a) exhibits decayed oscillation behavior. To explore the physical mechanism, we consider the high-frequency ($1/\tau\ll\omega_0$, $eE_Dd\ll\hbar\omega_0$) regime. In this case, the $m = 0$ term in the summation of Eq. (19) plays a dominant role, and the current expression reduces to

$$\langle j\rangle = \frac{2egv_F}{\pi}\frac{eE_Dd\hbar/\tau}{(\hbar/\tau)^2+(eE_Dd)^2}J_0^2\left(\frac{eE_Ad}{\hbar\omega_0}\right) = \langle j\rangle|_{E_A=0}J_0^2(\bar{\omega}_A). \tag{21}$$

Two interesting features can be observed from Eq. (21).

(i) In the high-frequency regime, the nonlinear current response to the dc field is modulated by the ac field in the same way [by a factor $J_0^2(\bar{\omega}_A)$] as that for the linear response, i.e., $\langle j\rangle_{\text{Linear}} = \frac{e^2 E_D v_F \tau}{4\pi^2 \hbar l_B^2} J_0^2(\bar{\omega}_A)$ (ac-field-modulated chiral anomaly effect).

(ii) The current vanishes when $J_0(\bar{\omega}_A) = 0$ corresponding to $\bar{\omega}_A = \frac{eE_A d}{\hbar\omega_0} = 2.40, 5.52, 8.65, \ldots$. This complete suppression of current is an effect known as dynamic localization.

Beyond the high-frequency regime, the higher-order terms in Eq. (19) cannot be ignored and the ac field has a different modulation effect [see the curves for $\bar{\omega}_D = 0.1$ and 1.0 in Fig. 3(a)].

Now we use the Floquet theory to gain a deeper understanding of the physical mechanism of dynamic localization, i.e., the vanishing of the current at certain values of ac field parameters $\bar{\omega}_A = eE_A d/\hbar\omega_0$. It is well known that the dynamics of a system with spatial periodic potential is determined by the energy band. Similarly, the dynamics of a system driven by a temporal periodic field is determined by the quasienergy. If the Hamiltonian of a system satisfies the periodic condition that $H(t) = H(t+T)$, the solutions corresponding to the Schrodinger equation may be written as a complete set of Floquet wave functions: $\psi_{\tilde{\varepsilon}}(t) = \exp(-i\tilde{\varepsilon}t)u_{\tilde{\varepsilon}}(t)$, where $\tilde{\varepsilon}$ is the so-called "quasienergy," and $u_{\tilde{\varepsilon}}(t) = u_{\tilde{\varepsilon}}(t+T)$ is also T-periodic [68–70]. In the high-frequency regime, the quasienergy of the system considered here is given by

$$\tilde{\varepsilon}_0^{\chi} = \frac{1}{T}\int_0^T dt\,\varepsilon_0^{\chi}(k,t), \tag{22}$$

where $\varepsilon_0^{\chi}(k,t) = -\chi\frac{\hbar v}{d}[\sin(\tilde{k}d)\pm b]$, with $\tilde{k} = k + \frac{eE_A}{\hbar\omega_0}\sin(\omega_0 t)$ being a time-dependent wave vector. In the following discussions, we choose $b = 0$ because b in $\varepsilon_0^{\chi}(k,t)$ only leads to a constant shift of the quasienergy. Thereby, one can obtain

$$\tilde{\varepsilon}_0^{\chi} = -\frac{\chi\hbar v}{d}\sin(kd)J_0(\bar{\omega}_A). \tag{23}$$

The quasienergy as a function of $\bar{\omega}_A = \frac{eE_A d}{\hbar\omega_0}$ is shown in Fig. 3(b). Comparing quasienergy [Eq. (23) and Fig. 3(b)] with the current at the high-frequency limit [Eq. (21) as well as Fig. 3(a)], one can clearly see that the band collapse and the disappearance of current occur under the same condition that $J_0(\bar{\omega}_A) = 0$. Physically, at the collapse points of the corresponding quasienergy, the "effective mass" of electrons becomes infinite, which leads to the dynamic localization and the vanishing of the current. Here one can see that the current response (related to chiral anomaly) and the (quasi)energy band are modulated in a way similar to that in topological trivial systems (like semiconductors). One of the effects of the ac field (in the high-frequency range) considered in our work is the renormalization/suppression of the quasienergy bandwidth and the associated modulation of the current response (related to chiral anomaly). This is remarkably different from the previous studies on the Floquet topological insulators and Floquet Weyl semimetals. For example, based on circularly polarized light fields, the dynamical gap opening in graphene [46–48], the generation of Weyl nodes from Dirac semimetals [52], and the shift of the positions of Weyl nodes [58] have been explored. Moreover, unlike previous research based on the linear dispersion, our present work focuses on the nonlinear response in the presence of strong fields, where the excitation beyond the low-energy linear dispersion is involved and a very different feature (from that based on the linear dispersion) occurs [61,67].

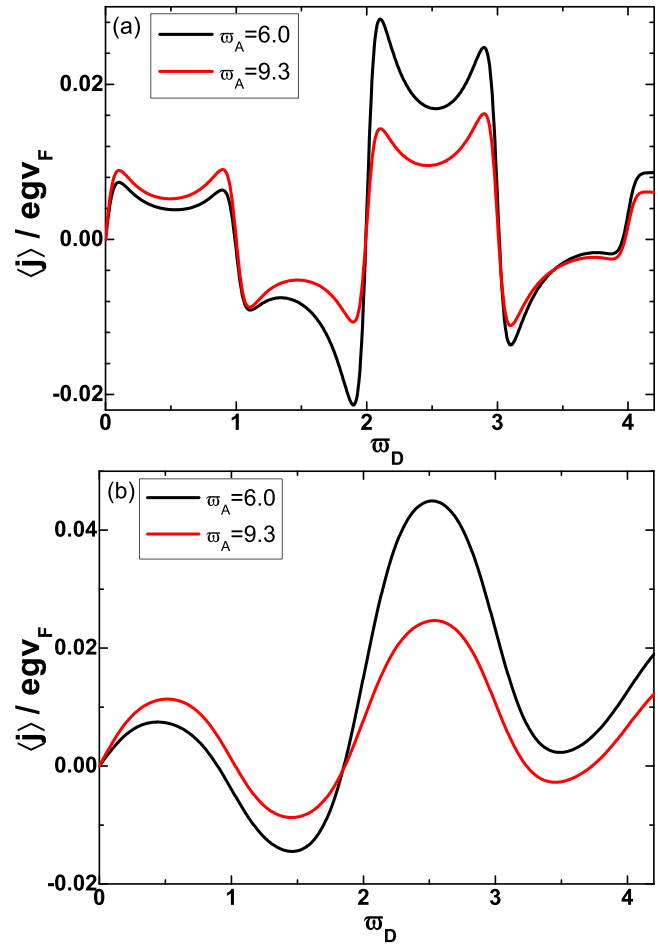

FIG. 4. The current (in units of egv_F) as a function of $\bar{\omega}_D$ with $\bar{\alpha} = 0.1$ in panel (a) and $\bar{\alpha} = 0.67$ in panel (b). The black and red lines correspond to $\bar{\omega}_A = 6.0$ and 9.3, respectively. The frequency of the cosinusoidal field is chosen as $\omega_0 = 0.6$ THz.

2. Nonlinear charge transport modulated by the cosinusoidal electric field II: Multiple photon-assisted transport

As discussed above, the $m = 0$ term [in Eq. (19)] dominates the contribution to the current in the high-frequency regime. Furthermore, a resonant peak, the so-called Esaki-Tsu peak, may appear in the current when the Bloch frequency matches the relaxation rate (i.e., $\bar{\omega}_D = \bar{\alpha}$) [71–73]. The other terms ($m\neq 0$) also have appreciable effects in the intermediate- or low-frequency regime. In particular, we notice that for the mth term, the local maximal value of the current $|\langle j\rangle|$ is achieved when $eE_D d = m\hbar\omega_0 \pm \hbar/\tau$ (i.e., $\bar{\omega}_D = m \pm \bar{\alpha}$), corresponding to the m-photon-assisted charge transport process. Typical results of the current $\langle j\rangle$ as a function of $\bar{\omega}_D$ are shown in Fig. 4 for several values of $\bar{\alpha}$ and $\bar{\omega}_A$. The peak or valley in the current curve (at $\bar{\omega}_D = m \pm \bar{\alpha}$), the generalization of the

Esaki-Tsu peak, can be clearly seen in Fig. 4(a). Moreover, we can observe from Fig. 4(a) that the corresponding amplitude of the current can be modulated by the ac field. In addition, we also notice from Fig. 4(b) that, with increasing $\bar{\alpha}$, the adjacent peaks or adjacent valleys embodied in current curves, corresponding to the m-photon process ($m\hbar\omega_0+\hbar/\tau$) and the $(m+1)$-photon process ($(m+1)\hbar\omega_0-\hbar/\tau$), respectively, may merge into one peak or one valley. For Weyl semimetals under an external magnetic field, the relaxation time τ due to various scattering processes actually depends on the magnetic field [28–32]. Therefore, by tuning the magnetic field (thus changing τ), it may be possible to experimentally observe the change of the current pattern related to the multiple-photon-assisted charge transport processes [the pattern of double peaks versus the pattern of a single peak between $m\hbar\omega_0$ and $(m+1)\hbar\omega_0$]. We would like to point out that the screening effect also affects the relaxation time [74,75]. It has an impact on the photon-assisted transport, while it does not affect the dynamic localization.

B. Nonlinear charge transport modulated by the pulsed field

Now, we turn to discuss nonlinear charge transport in Weyl semimetals modulated by a periodic pulsed field $\boldsymbol{E}_A = E_A P(\omega_0 t)\hat{z}$, where $P(\omega_0 t)$ is expressed as Eq. (7). The corresponding current for the case at zero temperature can be analytically derived and the final result is given by

$$\langle j\rangle = 2\frac{egv_F\bar{\alpha}}{\pi}\,\mathrm{Im}\left(\frac{1}{\bar{\alpha}-i\bar{\omega}_D}\right)-8\frac{egv_F\bar{\alpha}}{\pi\bar{T}_0}\sin^2\bar{\omega}_A \times \mathrm{Im}\left[\frac{1}{(\bar{\alpha}-i\bar{\omega}_D)^2}\frac{e^{\frac{(\bar{\alpha}-i\bar{\omega}_D)\bar{T}_0}{2}}-1}{e^{\frac{(\bar{\alpha}-i\bar{\omega}_D)\bar{T}_0}{2}}+1}\right], \tag{24}$$

where $\bar{T}_0 = 2\pi$ denotes the period of the ac field. The detailed derivation of Eq. (24) is presented in the Appendix. It is clear that in the presence of a periodic pulsed field the current [Eq. (24)] is remarkably different from that for the trigonometric ac field [Eq. (19)].

Herein, we briefly discuss the current response in the presence of a periodic pulsed field. There are several points that need to be noted.

(i) When $E_D = 0$, i.e., $\bar{\omega}_D = 0$, one can find that $\langle j\rangle = 0$.

(ii) When $E_A\to 0$, i.e., $\bar{\omega}_A\to 0$, we have $\langle j\rangle\to\frac{2egv_F}{\pi}\frac{\bar{\alpha}\bar{\omega}_D}{\bar{\alpha}^2+\bar{\omega}_D^2}$, which is just the result for the case in the presence of a pure dc field, with a Esaki-Tsu peak in the current response curve.

(iii) With an increasing ac field, more peaks may appear as shown in Fig. 5. Interestingly, the effect from the ac field disappears when $\bar{\omega}_A = m\pi$ (m an integer). As an example, the currents for $\bar{\omega}_A = 0$ and $\bar{\omega}_A = 3\pi$ are identical (shown as the black curve and the blue curve in Fig. 5). The frequency/period of the ac field also has an important impact on the current response. We also plot in Fig. 6 the long-time averaged current $\langle j\rangle$ as a function of the strength of the dc field $\omega_D = eE_D d$ with different ac field frequencies. From Fig. 6, one can see that different current response patterns appear when changing the frequency of the ac field.

(iv) In the high-frequency regime, the current reduces to the neat form $\langle j\rangle\to\frac{2egv_F}{\pi}\frac{\bar{\alpha}\bar{\omega}_D}{\bar{\alpha}^2+\bar{\omega}_D^2}\cos^2\bar{\omega}_A$, which indicates the dynamic localization again under the condition of $\cos\bar{\omega}_A = 0$.

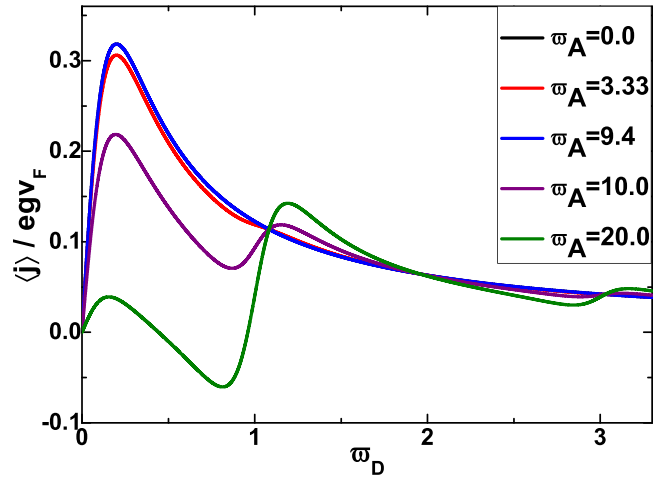

FIG. 5. The current response $\langle j\rangle$ (in units of egv_F) as a function of $\bar{\omega}_D$ for the periodic pulsed fields with different field strengths ($\bar{\omega}_A$). The parameters are chosen as $\omega_0 = 0.6$ THz, $\bar{\alpha} = 0.2$, and $\bar{\omega}_A = 0$, 3.33, 9.4, 10.0, and 20.0. The curves for $\bar{\omega}_A = 0$ (black curve) and $\bar{\omega}_A = 9.4$ (blue curve) overlap.

Different from the case of an ac field in the form of a trigonometric function, the dynamic localization appears periodically with changing the amplitude of the pulsed field, i.e., $\bar{\omega}_A = (2m+1)\pi/2$, with m being an integer. The locations of $\langle j\rangle = 0$ in the current curve in this case should also correspond to the collapse points of the quasienergy. According to Eq. (22), one can obtain the quasienergy in the periodic pulsed field in the high-frequency regime as

$$\tilde{\varepsilon}_{0,\chi} = -\frac{2\chi\hbar v}{d}\sin(kd)\cos\left(\frac{eE_A d}{\hbar\omega_0}\right). \tag{25}$$

The quasienergy collapse points, i.e., the points satisfying $\cos(\frac{eE_A d}{\hbar\omega_0}) = 0$, are just the points for the occurrence of dynamic localization ($\langle j\rangle = 0$).

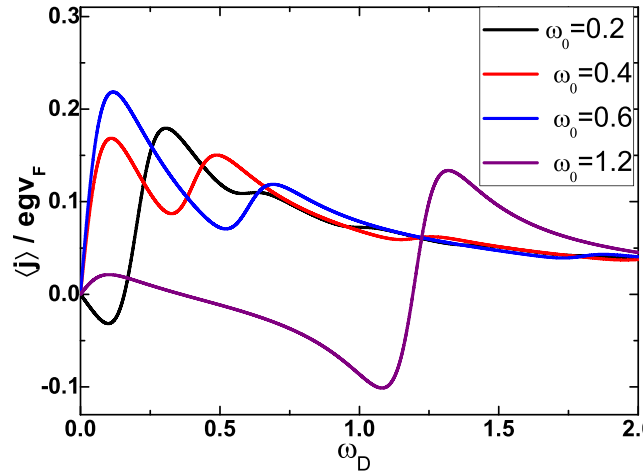

FIG. 6. The current response $\langle j\rangle$ (in units of egv_F) as a function of $\omega_D = eE_D d$ for the periodic pulsed field with various frequencies ω_0. The black, red, blue, and purple curves correspond to $\omega_0 = 0.2$, 0.4, 0.6, and 1.2 THz, respectively. Other parameters are chosen as $\omega_A = eE_A d = 6$ THz and $1/\tau = 0.12$ THz.

Our theoretical studies have revealed several interesting features of the nonlinear charge transport modulated by ac fields in Weyl semimetals, such as the suppression of current due to dynamic localization, the multiple-photon-assisted transport and the associated different patterns of current curves. At the end of this paper, we briefly discuss the experimental conditions to observe the above theoretical predictions and explain how to choose the physical parameters. For the typical type-I Weyl semimetal material TaAs [5], the lattice constants are $a = b = 3.437$ Åand $c = 11.656$ Å. As a rough estimation, we choose $\tau \sim 10^{-12}$ s and $d \sim 5$ Å. Then, the critical external electric field between the linear response and the nonlinear response is estimated as $E^c = \frac{\hbar}{ed\tau} \sim 1.3 \times 10^6$ V/m. The strong magnetic field condition in this paper requests that $\hbar v/l_B > eE_D d$. We suppose $v = 3 \times 10^5$ m/s and the required magnetic field $B = 0.73$ T, which corresponds to $l_B = 3.0 \times 10^{-7}$ m. In order to observe the influence of the ac field in experiment, especially the behavior of the current entirely disappearing around the first quasienergy collapse point for $J_0(\frac{eE_A d}{\hbar\omega_0}) = 0$, one can choose $E_A = 2 \times 10^6$ V/m and $\omega_0 = 0.63$ THz. The experimental conditions estimated above are easily realized in the current THz experiments related to condensed-matter physics. Therefore, we hope that the theoretical findings in this work could be experimentally observed in the near future.

IV. SUMMARY

In this paper we theoretically investigated the nonlinear charge transport of Weyl semimetals in the presence of dc-ac fields in the ultraquantum regime. Nonperturbative calculations based on the SLE have revealed the key characters of the ac-field-modulated charge transport. Under an external dc-ac field with the ac field $\boldsymbol{E}_A = E_A \cos(\omega_0 t)$, dynamic localization and quasienergy band collapse occur under a suitable condition of $J_0(\bar{\omega}_A) = 0$ in the high-frequency regime. While in the intermediate- and low-frequency regimes, the multiple-photon-assisted transport process modulated by the cosinusoidal field leads to magnetic-field-tunable resonant current peaks, which are the extension of the Esaki-Tsu peak. The position and the amplitude of the peaks can be tuned by the magnetic field and the ac field. The case with a periodic pulsed field, i.e., $\boldsymbol{E}_A = 2E_A \sum_{m=0}^{\infty}(-1)^m \delta(\omega_0 t - m\pi)$, has also been studied, which shows similar ac-field-induced dynamic localization and quasienergy band collapse under a different condition of $\cos\bar{\omega}_A = 0$. In addition, we have also found that the influence of the periodic pulsed field on current may vanish when $\bar{\omega}_A = m\pi$, with m being an integer. Our theoretical results deepen the understanding of the nonlinear transport properties of Weyl semimetals and provide helpful guidance for the design of photoelectric devices based on topological materials.

ACKNOWLEDGMENTS

This work was supported by the National Key Research and Development Program of China (Grant No. 2017YFA 0303400), the NSFC-RGC (Grant No. 11861161002), and the National Natural Science Foundation of China (Grants No. 12174032, No. 11774036, No. 12174033, No. 12175023, and No. 11625415).

APPENDIX

In this Appendix, we present the details of deriving the current response, i.e., Eq. (24), in the presence of a periodic pulsed field. Substituting Eqs. (5), (7), (13), and (16) into Eq. (15), the long-time averaged current is derived as $\langle j \rangle = egv_F J_2$, where

$$J_2 = \lim_{N\to\infty} \frac{\bar{\alpha}}{2\pi} \frac{1}{N\bar{T}_0} \sum_{m=0}^{N-1} G_m, \tag{A1}$$

with

$$G_m = \int_{m\bar{T}_0}^{(m+1)\bar{T}_0} d\bar{t} \int_0^{\bar{t}} d\bar{t}' Z(\bar{t}, \bar{t}'). \tag{A2}$$

G_m can be divided into two parts,

$$G_m = G_m^A + G_m^B, \tag{A3}$$

where

$$G_m^A = \int_{m\bar{T}_0}^{\left(m+\frac{1}{2}\right)\bar{T}_0} d\bar{t} \int_0^{\bar{t}} d\bar{t}' Z(\bar{t}, \bar{t}') \tag{A4}$$

and

$$G_m^B = \int_{\left(m+\frac{1}{2}\right)\bar{T}_0}^{(m+1)\bar{T}_0} d\bar{t} \int_0^{\bar{t}} d\bar{t}' Z(\bar{t}, \bar{t}'). \tag{A5}$$

After some derivations, we have $G_m^A = \int_{m\bar{T}_0}^{(m+\frac{1}{2})\bar{T}_0} g_m^A d\bar{t}$ and $G_m^B = \int_{(m+\frac{1}{2})\bar{T}_0}^{(m+1)\bar{T}_0} g_m^B d\bar{t}$, where

$$g_m^{A(B)} = \left[\sum_{n=0}^{m-1}\left(\int_{n\bar{T}_0}^{\left(n+\frac{1}{2}\right)\bar{T}_0} d\bar{t}' + \int_{\left(n+\frac{1}{2}\right)\bar{T}_0}^{(n+1)\bar{T}_0} d\bar{t}'\right) + \int_{m\bar{T}_0}^{\bar{t}} d\bar{t}'\right] \times Z(\bar{t}, \bar{t}') = \sum_{n=0}^{m-1}\left[\left(g_m^{A(B)}\right)_n^{(1)} + \left(g_m^{A(B)}\right)_n^{(2)}\right] + \left(g_m^{A(B)}\right)^{(3)}. \tag{A6}$$

By using the periodic property of $f(\bar{t})$, one can obtain

$$\left(g_m^A\right)_n^{(1)} = 4\,\mathrm{Im}\left[\frac{e^{-(\bar{\alpha}-i\bar{\omega}_D)(\bar{t}-n\bar{T}_0)}}{\bar{\alpha}-i\bar{\omega}_D}\left(e^{\frac{(\bar{\alpha}-i\bar{\omega}_D)\bar{T}_0}{2}} - 1\right)\right], \tag{A7}$$

$$\left(g_m^A\right)_n^{(2)} = 4\,\mathrm{Im}\left[\frac{e^{-(\bar{\alpha}-i\bar{\omega}_D)(\bar{t}-n\bar{T}_0)}}{\bar{\alpha}-i\bar{\omega}_D}\left(e^{\frac{(\bar{\alpha}-i\bar{\omega}_D)\bar{T}_0}{2}} - 1\right)e^{\frac{(\bar{\alpha}-i\bar{\omega}_D)\bar{T}_0}{2}} e^{i2\bar{\omega}_A}\right], \tag{A8}$$

$$\left(g_m^A\right)^{(3)} = 4\,\mathrm{Im}\left[\frac{1}{\bar{\alpha}-i\bar{\omega}_D} - \frac{e^{-(\bar{\alpha}-i\bar{\omega}_D)(\bar{t}-m\bar{T}_0)}}{\bar{\alpha}-i\bar{\omega}_D}\right], \tag{A9}$$

$$\left(g_m^B\right)_n^{(1)} = 4\,\mathrm{Im}\left[\frac{e^{-(\bar{\alpha}-i\bar{\omega}_D)(\bar{t}-n\bar{T}_0)}}{\bar{\alpha}-i\bar{\omega}_D}\left(e^{\frac{\left(\bar{\alpha}-i\bar{\omega}_D\right)\bar{T}_0}{2}}-1\right)e^{-i2\bar{\omega}_A}\right], \tag{A10}$$

$$\left(g_m^B\right)_n^{(2)} = 4\,\mathrm{Im}\left[\frac{e^{-(\bar{\alpha}-i\bar{\omega}_D)(\bar{t}-n\bar{T}_0)}}{\bar{\alpha}-i\bar{\omega}_D}\left(e^{\frac{\left(\bar{\alpha}-i\bar{\omega}_D\right)\bar{T}_0}{2}}-1\right)e^{\frac{(\bar{\alpha}-i\bar{\omega}_D)\bar{T}_0}{2}}\right], \tag{A11}$$

$$\left(g_m^B\right)^{(3)} = 4\,\mathrm{Im}\left[\frac{1}{\bar{\alpha}-i\bar{\omega}_D}-\frac{e^{-(\bar{\alpha}-i\bar{\omega}_D)(\bar{t}-m\bar{T}_0)}}{\bar{\alpha}-i\bar{\omega}_D}e^{\frac{(\bar{\alpha}-i\bar{\omega}_D)\bar{T}_0}{2}} + \frac{e^{-(\bar{\alpha}-i\bar{\omega}_D)(\bar{t}-m\bar{T}_0)}}{\bar{\alpha}-i\bar{\omega}_D}\left(e^{\frac{\left(\bar{\alpha}-i\bar{\omega}_D\right)\bar{T}_0}{2}}-1\right)e^{-i2\bar{\omega}_A}\right]. \tag{A12}$$

In the above equations, $\bar{T}_0 = 2\pi$. Substituting these equations into Eq. (A1), one can finally arrive at Eq. (24).

[1] A. H. Castro Neto, F. Guinea, N. M. R. Peres, K. S. Novoselov, and A. K. Geim, The electronic properties of graphene, Rev. Mod. Phys. **81**, 109 (2009).

[2] S. Das Sarma, Shaffique Adam, E. H. Hwang, and Enrico Rossi, Electronic transport in two-dimensional graphene, Rev. Mod. Phys. **83**, 407 (2011).

[3] M. Z. Hasan and C. L. Kane, Colloquium: Topological insulators, Rev. Mod. Phys. **82**, 3045 (2010).

[4] X. L. Qi and S. C. Zhang, Topological insulators and superconductors, Rev. Mod. Phys. **83**, 1057 (2011).

[5] N. P. Armitage, E. J. Mele, and A. Vishwanath, Weyl and Dirac semimetals in three-dimensional solids, Rev. Mod. Phys. **90**, 015001 (2018), and references therein.

[6] X. Wan, A. M. Turner, A. Vishwanath, and S. Y. Savrasov, Topological semimetal and Fermi-arc surface states in the electronic structure of pyrochlore iridates, Phys. Rev. B **83**, 205101 (2011).

[7] A. A. Burkov and L. Balents, Weyl Semimetal in a Topological Insulator Multilayer, Phys. Rev. Lett. **107**, 127205 (2011).

[8] G. Xu, H. Weng, Z. Wang, X. Dai, and Z. Fang, Chern Semimetal and the Quantized Anomalous Hall Effect in $HgCr_2Se_4$, Phys. Rev. Lett. **107**, 186806 (2011).

[9] P. Hosur, S. A. Parameswaran, and A. Vishwanath, Charge Transport in Weyl Semimetals, Phys. Rev. Lett. **108**, 046602 (2012).

[10] C. Fang, M. J. Gilbert, X. Dai, and B. A. Bernevig, Multi-Weyl Topological Semimetals Stabilized by Point Group Symmetry, Phys. Rev. Lett. **108**, 266802 (2012).

[11] C. X. Liu, P. Ye, and X. L. Qi, Chiral gauge field and axial anomaly in a Weyl semimetal, Phys. Rev. B **87**, 235306 (2013).

[12] H. Weng, C. Fang, Z. Fang, B. A. Bernevig, and X. Dai, Weyl Semimetal Phase in Noncentrosymmetric Transition-Metal Monophosphides, Phys. Rev. X **5**, 011029 (2015).

[13] A. A. Soluyanov, D. Gresch, Z. Wang, Q. Wu, M. Troyer, X. Dai, and B. A. Bernevig, Type-II Weyl semimetals, Nature (London) **527**, 495 (2015).

[14] X.-P. Li, K. Deng, B. Fu, Y.K. Li, D.-S. Ma, J.F. Han, J. Zhou, S. Zhou, and Y. Yao, Type-III Weyl semimetals: $(TaSe_4)_2I$, Phys. Rev. B **103**, L081402 (2021).

[15] L. Chen and K. Chang, Chiral-Anomaly-Driven Casimir-Lifshitz Torque between Weyl Semimetals, Phys. Rev. Lett. **125**, 047402 (2020).

[16] J.-N. Rong, L. Chen, and K. Chang, Chiral anomaly-enhanced Casimir interaction between Weyl semimetals, Chinese Phys. Lett. **38**, 084501 (2021).

[17] G. Sharma, P. Goswami, and S. Tewari, Nernst and magnetothermal conductivity in a lattice model of Weyl fermions, Phys. Rev. B **93**, 035116 (2016).

[18] Y. Sun and A. Wang, Magneto-optical conductivity of double Weyl semimetals, Phys. Rev. B **96**, 085147 (2017).

[19] Y. Gao, F. Zhang, W. Zhang, Four-wave mixing of Weyl semimetals in a strong magnetic field, J. Phys.: Condens. Matter **32**, 275502 (2020).

[20] C. M. Wang, H.-P. Sun, H.-Z. Lu, and X. C. Xie, 3D Quantum Hall Effect of Fermi Arcs in Topological Semimetals, Phys. Rev. Lett. **119**, 136806 (2017).

[21] Z. Zheng, Z. Lin, D.-W. Zhang, S.-L. Zhu, and Z. D. Wang, Chiral magnetic effect in three-dimensional optical lattices, Phys. Rev. Research **1**, 033102 (2019).

[22] J. C. de Boer, D. H. Wielens, J. A. Voerman, B. de Ronde, Y. Huang, M. S. Golden, C. Li, and A. Brinkman, Nonlocal signatures of the chiral magnetic effect in the Dirac semimetal $Bi_{0.97}Sb_{0.03}$, Phys. Rev. B **99**, 085124 (2019).

[23] U. Dey, S. Nandy, and A. Taraphder, Dynamic chiral magnetic effect and anisotropic natural optical activity of tilted Weyl semimetals, Sci. Rep. **10**, 2699 (2020).

[24] A. Menon, S. Chattopadhay, and B. Basu, Chiral magnetic effect in lattice models of tilted multi-Weyl semimetals, Phys. Rev. B **104**, 075129 (2021).

[25] I. Sodemann and L. Fu, Quantum Nonlinear Hall Effect Induced by Berry Curvature Dipole in Time-Reversal Invariant Materials, Phys. Rev. Lett. **115**, 216806 (2015).

[26] Y Gao, F. Zhang, and W. Zhang, Phys. Second-order nonlinear Hall effect in Weyl semimetals, Phys. Rev. B **102**, 245116 (2020).

[27] Z. Z. Du, C. M. Wang, H.-P. Sun, H.-Z. Lu, and X. C. Xie, Quantum theory of the nonlinear Hall effect, Nat. Commun. **12**, 5038 (2021).

[28] B. Z. Spivak and A. V. Andreev, Magnetotransport phenomena related to the chiral anomaly in Weyl semimetals, Phys. Rev. B **93**, 085107 (2016).

[29] X. Huang, H. Geng, and L. Sheng, Magnetic-field-dependent intervalley relaxation time in Weyl semimetals, Phys. Rev. B **103**, 115208 (2021).

[30] V. Aji, Adler-Bell-Jackiw anomaly in Weyl semimetals: Application to pyrochlore iridates, Phys. Rev. B **85**, 241101(R) (2012).

[31] H.-Z. Lu, S.-B. Zhang, and S.-Q. Shen, High-field magnetoconductivity of topological semimetals with short-range potential, Phys. Rev. B **92**, 045203 (2015).

[32] P. Goswami, J. H. Pixley, and S. Das Sarma, Axial anomaly and longitudinal magnetoresistance of a generic three-dimensional metal, Phys. Rev. B **92**, 075205 (2015).

[33] F. D. M. Haldane, Berry Curvature on the Fermi Surface: Anomalous Hall Effect as a Topological Fermi-Liquid Property, Phys. Rev. Lett. **93**, 206602 (2004).

[34] D. Xiao, Y. Yao, Z. Fang, and Q. Niu, Berry-Phase Effect in Anomalous Thermoelectric Transport, Phys. Rev. Lett. **97**, 026603 (2006).

[35] Y.-W. Wei, C.-K. Li, J. Qi, and J. Feng, Magnetoconductivity of type-II Weyl semimetals, Phys. Rev. B **97**, 205131 (2018).

[36] G. Sharma, P. Goswami, and S. Tewari, Chiral anomaly and longitudinal magnetotransport in type-II Weyl semimetals, Phys. Rev. B **96**, 045112 (2017).

[37] M. Trescher, E. J. Bergholtz, and J. Knolle, Quantum oscillations and magnetoresistance in type-II Weyl semimetals: Effect of a field-induced charge density wave, Phys. Rev. B **98**, 125304 (2018).

[38] H. B. Nielsen and M. Ninomiya, The Adler-Bell-Jackiw anomaly and Weyl fermions in a crystal, Phys. Lett. B **130**, 389 (1983).

[39] D. T. Son and B. Z. Spivak, Chiral anomaly and classical negative magnetoresistance of Weyl metals, Phys. Rev. B **88**, 104412 (2013).

[40] K.-S. Kim, H.-J. Kim, and M. Sasaki, Boltzmann equation approach to anomalous transport in a Weyl metal, Phys. Rev. B **89**, 195137 (2014).

[41] M. Novak, S. Sasaki, K. Segawa, and Y. Ando, Large linear magnetoresistance in the Dirac semimetal TlBiSSe, Phys. Rev. B **91**, 041203(R) (2015).

[42] N. Ramakrishnan, M. Milletari, and S. Adam, Transport and magnetotransport in three-dimensional Weyl semimetals, Phys. Rev. B **92**, 245120 (2015).

[43] X. Huang, L. Zhao, Y. Long, P. Wang, D. Chen, Z. Yang, H. Liang, M. Xue, H. Weng, Z. Fang, X. Dai, and G. Chen, Observation of the Chiral-Anomaly-Induced Negative Magnetoresistance in 3D Weyl Semimetal TaAs, Phys. Rev. X **5**, 031023 (2015).

[44] C.-L. Zhang, S.-Y. Xu, I. Belopolski, Z. Yuan, Z. Lin, B. Tong, G. Bian, N. Alidoust, C.-C. Lee, S.-M. Huang *et al.*, Signatures of the Adler–Bell–Jackiw chiral anomaly in a Weyl fermion semimetal, Nat. Commun. **7**, 10735 (2016).

[45] M.-X. Deng, G. Y. Qi, R. Ma, R. Shen, R.-Q. Wang, L. Sheng, and D. Y. Xing, Quantum Oscillations of the Positive Longitudinal Magnetoconductivity: A Fingerprint for Identifying Weyl Semimetals, Phys. Rev. Lett. **122**, 036601 (2019).

[46] T. Oka and H. Aoki, Photovoltaic Hall effect in graphene, Phys. Rev. B **79**, 081406(R) (2009).

[47] H. L. Calvo, H. M. Pastawski, S. Roche, and L. E. F. Foa Torres, Tuning laser-induced band gaps in graphene, Appl. Phys. Lett. **98**, 232103 (2011).

[48] T. Kitagawa, T. Oka, A. Brataas, L. Fu, and E. Demler, Transport properties of nonequilibrium systems under the application of light: Photoinduced quantum Hall insulators without Landau levels, Phys. Rev. B **84**, 235108 (2011).

[49] Q. Ma, S.-Y. Xu, C.-K. Chan, C.-L. Zhang, G. Chang, Y. Lin, W. Xie, T. Palacios, H. Lin, S. Jia, P. A. Lee, P. Jarillo-Herrero, and N. Gedik, Direct optical detection of Weyl fermion chirality in a topological semimetal, Nat. Phys. **13**, 842 (2017).

[50] C.-K. Chan, N. H. Lindner, G. Refael, and P. A. Lee, Photocurrents in Weyl semimetals, Phys. Rev. B **95**, 041104(R) (2017).

[51] Ya. I. Rodionov, K. I. Kugel, and F. Nori, Floquet spectrum and driven conductance in Dirac materials: Effects of Landau-Zener-Stückelberg-Majorana interferometry, Phys. Rev. B **94**, 195108 (2016).

[52] H. Hübener, M. A. Sentef, U. De Giovannini, A. F. Kemper, and Angel Rubio, Creating stable Floquet-Weyl semimetals by laser-driving of 3D Dirac materials, Nat. Commun. **8**, 13940 (2017).

[53] L. Bucciantini, S. Roy, S. Kitamura, and Takashi Oka, Emergent Weyl nodes and Fermi arcs in a Floquet Weyl semimetal, Phys. Rev. B **96**, 041126(R) (2017).

[54] R. Chen, B. Zhou, and D.-H. Xu, Floquet Weyl semimetals in light-irradiated type-II and hybrid line-node semimetals, Phys. Rev. B **97**, 155152 (2018).

[55] R. Chen, D.-H. Xu, and B. Zhou, Floquet topological insulator phase in a Weyl semimetal thin film with disorder, Phys. Rev. B **98**, 235159 (2018).

[56] M. Umer, R. W. Bomantara, and J. Gong, Dynamical characterization of Weyl nodes in Floquet Weyl semimetal phases, Phys. Rev. B **103**, 094309 (2021).

[57] W. Zhu, M. Umer, and J. Gong, Floquet higher-orderWeyl and nexus semimetals, Phys. Rev. Research **3**, L032026 (2021).

[58] A. Menon, D. Chowdhury, and B. Basu, Photoinduced tunable anomalous Hall and Nernst effects in tilted Weyl semimetals using Floquet theory, Phys. Rev. B **98**, 205109 (2018).

[59] J. Yang, D.-F. Shao, S.-H. Zhang, and W. Yang, Friedel oscillations in graphene gapped by breaking $\mathcal{P}$ and $\mathcal{T}$ symmetries: Topological and geometrical signatures of electronic structure, Phys. Rev. B **104**, 035402 (2021).

[60] A. Kundu, H. A. Fertig, and B. Seradjeh, Effective Theory of Floquet Topological Transitions, Phys. Rev. Lett. **113**, 236803 (2014).

[61] Z. Wang, Z. Fu, P. Zhang, X.-G. Zhao, and W. Zhang, Nonlinear current response of Weyl semimetals in the ultraquantum regime, Phys. Rev. B **101**, 245313 (2020).

[62] V. M. Kenkre and D. W. Brown, Exact solution of the stochastic Liouville equation and application to an evaluation of the neutron scattering function, Phys. Rev. B **31**, 2479 (1985).

[63] D. H. Dunlap and V. M. Kenkre, Effect of scattering on the dynamic localization of a particle in a time-dependent electric field, Phys. Rev. B **37**, 6622 (1988).

[64] X.-G. Zhao, W.-X. Yan, and D. W. Hone, Zener transitions between dissipative Bloch bands, Phys. Rev. B **57**, 9849 (1998).

[65] X.-G. Zhao and D. W. Hone, Zener transitions between dissipative Bloch bands. II. Current response at finite temperature, Phys. Rev. B **62**, 5010 (2000).

[66] D. Suqing, W. Zhang, and X. G. Zhao, Current response of two-band superlattices at finite temperatures, Phys. Rev. B **62**, 9943 (2000).

[67] M. M. Vazifeh and M. Franz, Electromagnetic Response of Weyl Semimetals, Phys. Rev. Lett. **111**, 027201 (2013).

[68] M. Holthaus and D. Hone, Quantum wells and superlattices in strong time-dependent fields, Phys. Rev. B **47**, 6499 (1993).

[69] M. Holthaus, Collapse of Minibands in Far-Infrared Irradiated Superlattices, Phys. Rev. Lett. **69**, 351 (1992).

[70] A. Gomez-Leon and G. Platero, Floquet-Bloch Theory and Topology in Periodically Driven Lattices, Phys. Rev. Lett. **110**, 200403 (2013).

[71] L. Esaki and R. Tsu, Superlattice and negative differential conductivity in semiconductors, IBM J. Res. Dev. **14**, 61 (1970).

[72] A. Wacker, Semiconductor superlattices: a model system for nonlinear transport, Phys. Rep. **357**, 1 (2002).

[73] K. Hwang, W.-R. Lee, and K. Park, Electric quantum oscillations in Weyl semimetals, Phys. Rev. Research **3**, 033132 (2021).

[74] X.-T. Ji, H.-Z. Lu, Z.-G. Zhu, and G. Su, Competition between the inter-valley scattering and the intra-valley scattering on magnetoconductivity induced by screened Coulomb disorder in Weyl semimetals, AIP Adv. **7**, 105003 (2017).

[75] X.-T. Ji, H.-Z. Lu, Z.-G. Zhu, and G. Su, Effect of the screened Coulomb disorder on magneto-transport in Weyl semimetals, J. Appl. Phys. **123**, 203901 (2018).